Identification of Two Distinct Electron Binding Motifs in the Anionic Water Clusters: A Vibrational Spectroscopic Study of the $(H_2O)_6^-$ Isomers

Nathan I. Hammer, Joseph R. Roscioli, and M. A. Johnson*

Sterling Chemistry Laboratory, Yale University, P.O. Box 208107, New Haven, Connecticut 06520

Received: April 25, 2005; In Final Form: June 13, 2005

Photoelectron spectroscopy of the water cluster anions, $(H_2O)_n^-$, has revealed that several isomeric forms are present for most sizes, and here, we use vibrational spectroscopy to address the structure of the $(H_2O)_6^-$ isomer that more weakly binds the extra electron. To overcome the severe line broadening that occurs in the OH stretching region of this isomer caused by fast electron autodetachment, we concentrate on the low-energy bending modes of the perdeutero isotopomer. Sharp spectroscopic signatures are recovered for two isomers using argon predissociation spectroscopy, and the resulting bands are heavily overlapped. To extract their independent contributions to the observed spectra, we exploit the substantial dependence of their relative populations on the number of attached argon atoms in the $(D_2O)_6^-\cdot Ar_m$ clusters, determined by photoelectron spectroscopy. The vibrational spectra of each isomer can then be isolated by spectral subtraction, which is implemented with a covariance mapping approach. The resulting band patterns establish that the more weakly binding isomer does not display the characteristic electron-binding motif common to the more strongly bound isomer class. Whereas the strongly binding isomer features a single water molecule pointing toward the excess electron cloud with both of its hydrogen atoms, the spectrum of the more weakly binding isomer suggests a structure where the electron is bound by a number of dangling OH groups corresponding to water molecules in acceptor−donor binding sites.

I. Introduction

Since their discovery in 1984,[1−3] the negatively charged water clusters, $(H_2O)_n^-$, have attracted much attention because of their potential to provide model systems with which to unravel how water networks deform to accommodate an excess electron. One of the primary motivations for this activity is to explore molecular-level aspects of the hydrated electron (e_{aq}^-),[4] an important intermediate in radiation-damaged biological systems.[5] Bowen and co-workers were the first to characterize the $(H_2O)_n^-$ clusters using photoelectron spectroscopy and interpreted isotopic shifts in the photoelectron spectra of $(H_2O)_6^-$ and $(H_2O)_7^-$ to indicate the presence of two isomers that differ in their electron-binding energies by about 0.3 eV.[6] Subsequent efforts[7−10] have established that such isomers are almost always present and can be roughly classified into three more-or-less continuously evolving groups according to their vertical electron detachment energies (VDEs) as indicated in Figure 1. These are labeled **I**, **II**, and **III** in decreasing order of their characteristic VDE values.

The trends established for small clusters have been recently observed to continue to very large sizes by variation of source conditions,[10] with isomers **II** and **III** being much more readily prepared in the $(D_2O)_n^-$ isotopomers.[10,11] The existence of a weak electron-binding class of clusters of large size has long been anticipated by theorists who have identified two different electron solvation morphologies according to whether the excess electron is localized in the interior or resides on the surface.[12] Thus, Neumark and co-workers[10] concluded that these more weakly bound species (**II** and **III**) were associated with surface-solvated electrons. Moreover, isomers **I** and **II** were shown to display different relaxation dynamics for two-photon photodetachment mediated by resonant excitation of the first electronically excited state,[10,13,14] such that the more strongly bound form

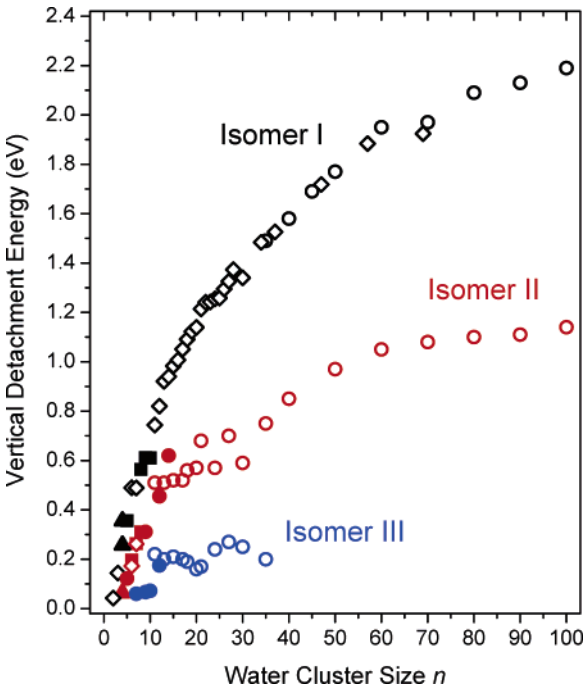

Figure 1. Summary of measured vertical electron detachment energies (VDE) of $(H_2O)_n^-$ clusters determined from their photoelectron spectra, which are sorted according to their classifications as different isomers: isomer **I** (black); isomer **II** (red); isomer **III** (blue). Data are a compilation from current study (filled circles), ref 7 (diamonds), ref 8 (squares), ref 9 (triangles), and ref 10 (open circles).

* Corresponding author. E-mail: mark.johnson@yale.edu.

10.1021/jp052144b CCC: $30.25
Published on Web 07/27/2005

exhibits the fastest decay rates. In fact, the size dependence of the relaxation rates found for **I** are observed to extrapolate to the fastest transients reported for e_{aq}^-.[15] In this paper, we manipulate the population of isomers **I** and **II** in the $n = 6$ cluster in order to isolate their independent band patterns in the low-energy, intramolecular bending region of the vibrational spectrum. This information is then used to elucidate key differences in the molecular-level accommodation motifs displayed by the two isomers.

The present paper capitalizes on our previous study,[16] where we identified the structures adopted by class **I** isomers of the $n = 4$, 5, and 6 clusters through a combined analysis of their intramolecular bending and OH stretching bands, observed with argon predissociation spectroscopy. Most importantly, all these structures were observed to display a common electron accommodation motif. In each case, one water molecule directs both of its hydrogen atoms toward the diffuse electron cloud and is attached to the associated network via a double H-bond acceptor (AA) arrangement. This unique water molecule was evidenced by its characteristic signatures in the OH stretching and intramolecular bending regions of the spectrum. In the stretching region, it contributes a dominant, strongly red-shifted doublet, split by about 100 cm^{-1}, in both the $(H_2O)_6^-$ and $(D_2O)_6^-$ spectra. The bending region provides an even more distinctive signature, as the AA water molecule yields a well-isolated, sharp band that is the only feature observed below the bending origin in the bare water molecule (1595 cm^{-1} in H_2O).

The earlier spectroscopic study[16] focused on isomer **I** because, with its higher binding energy, sharp bands are recovered in both the stretching and bending regions. On the other hand, isomer **II** binds the electron so weakly (VDE = 1500 cm^{-1}) that both the stretching (3400 cm^{-1}) and bending (1600 cm^{-1}) transitions of the $(H_2O)_6^-$ isotopomer occur above the onset of its vertical detachment continuum. As a result, the vibrational contributions of **II** are so severely broadened by autodetachment that they cannot be used for spectroscopic analysis, a circumstance that allowed the sharper band structures associated with **I** to be recorded without interference from **II**. We now exploit the known signature of **I** to isolate the spectrum of **II**. We concentrate on the $(D_2O)_6^-$ isotopomer in the bending region, because the fundamentals occur near 1200 cm^{-1}, sufficiently below the VDE of $n = 6$ (1500 cm^{-1}) to yield sharp bands, while the OD stretches of **II** occur too high (2500 cm^{-1}) to be of value. The relative populations of the two isomeric forms are found to strongly depend on the number of attached argon atoms in the $(D_2O)_6^-\cdot Ar_m$ series, and we quantify the argon-dependent population distribution using photoelectron spectroscopy. This information then allows deconvolution of the overlapping contributions to the bending spectra and thus isolation of the spectroscopic signature of isomer **II**.

II. Experimental Section

Vibrational spectra were acquired by predissociation of the size-selected $(D_2O)_6^-\cdot Ar_m$ complexes

$$(D_2O)_6^-\cdot Ar_m + h\nu \rightarrow (D_2O)_6^-\cdot Ar_{m-p} + pAr \qquad (1)$$

using a double-focusing, tandem time-of-flight mass spectrometer described previously.[17] The $(D_2O)_6^-\cdot Ar_m$ ($m = 0-10$) cluster ions were generated by slow secondary-electron attachment to argon-solvated neutral water clusters, where the slow electrons were prepared by ionizing a pulsed nozzle (Parker-Hannefin) expansion with a 1 keV counterpropagating electron beam. The expansion was formed by passing 4 atm of Ar carrier gas, saturated with water vapor over a reservoir held at 2 °C, through a 0.5 mm orifice. The clusters were irradiated with a tabletop IR laser source (Laser Vision) in the 1000−1600 cm^{-1} region, which was generated by parametric conversion in $AgGaSe_2$. Photoexcitation at 1200 cm^{-1} resulted in the loss of 3 Ar atoms from the larger clusters. The reported spectra result from the addition of approximately 20 individual scans and are corrected for laser pulse energy changes over the scan range. For photoelectron spectra, photodetachment was carried out with the fundamental beam from a Nd:YAG laser, and the resulting photoelectrons were analyzed with a field-free, time-of-flight photoelectron spectrometer.[18] Spectra typically resulted from 20 000 shots and were obtained with the laser polarization oriented along the electron flight axis.

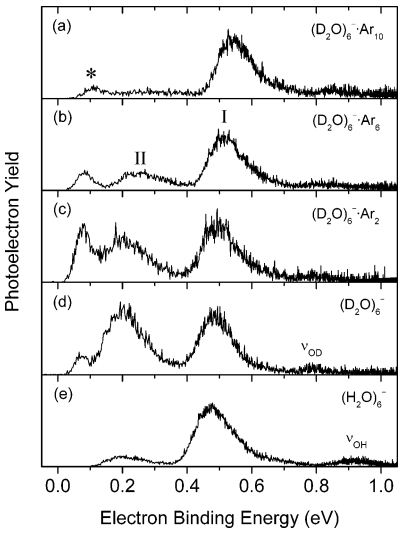

Figure 2. Photoelectron spectra of $(D_2O)_6^-\cdot Ar_m$; $m =$ (a) 10, (b) 6, (c) 2, (d) 0, and (e) $(H_2O)_6^-$. The asterisk indicates contamination from mass-degenerate $(D_2O)_2^-\cdot Ar_{m+2}$ clusters. The labels ν_{OH} and ν_{OD} correspond to excitations of the OH and OD stretching fundamentals, respectively.

III. Results and Discussion

III.1. Photoelectron Spectroscopy: Determination of the Isomer Populations in the $(D_2O)_6^-\cdot Ar_m$ Clusters. Figure 2 presents photoelectron spectra of $(D_2O)_6^-\cdot Ar_m$ ($m = 0$, 2, 6, and 10) along with that of $(H_2O)_6^-$, displayed in the bottom panel. Note that the low-binding feature at ~80 meV in the $(D_2O)_6^-\cdot Ar_m$ spectra (marked with an asterisk) is attributed to the mass-degenerate (at our resolution), very weakly bound $(D_2O)_2^-\cdot Ar_{m+2}$ clusters.[19] The origin bands corresponding to isomers **I** and **II**, originally identified by Coe et al.,[6,7] are indicated, where the envelope from the more strongly bound isomer includes isotope-dependent vibrational contributions from the hydrogen stretching modes (labeled ν_{OD} and ν_{OH} in traces 2d and 2e, respectively). The VDEs of both isomers shift to higher energy with increasing m by about 5 meV/Ar.

Although the two isomers contribute about equally to the bare $(D_2O)_6^-$ cluster ion ensemble (Figure 2d), the relative contribution from the lower-binding isomer (**II**) decreases by about a factor of 10 upon the addition of ten argon atoms. A similar suppression of the isomer **II** contribution with argon solvation was observed previously in both the $(H_2O)_6^-$ and $(H_2O)_8^-$ species.[8] This dramatic modulation of the isomer production ratio is key to the present study, as the $m = 10$ vibrational spectrum (Figure 3b) should primarily contain features arising from isomer **I**, and new peaks due to isomer **II** can then be systematically introduced by reducing the number of attached

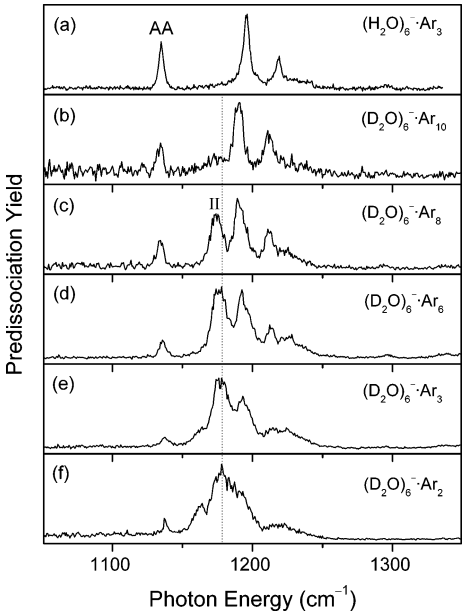

Figure 3. Argon predissociation spectra in the water bending region of (a) $(H_2O)_6^-\cdot Ar_3$ (photon energy scaled by 0.739), and $(D_2O)_6^-\cdot Ar_m$; m = (b) 10, (c) 8, (d) 6, (e) 3, and (f) 2. The dotted line corresponds to the location of the free D_2O bend fundamental (1178 cm^{-1}), and the AA label denotes the signature band arising from a water molecule in a double H-bond acceptor site. The label II (trace 2c) identifies the dominant band associated with isomer **II**.

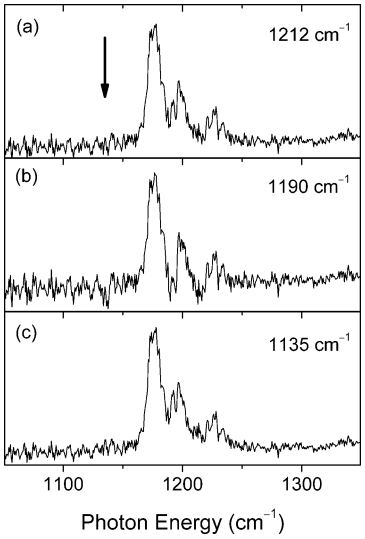

Figure 4. Spectrum of isomer **II**, obtained by subtracting the contribution from isomer **I** (isolated in the $(D_2O)_6^-\cdot Ar_{10}$ spectrum) from that of $(D_2O)_6^-\cdot Ar_6$, after normalizing the two spectra to the isomer **I** peaks at (a) 1212 cm^{-1}, (b) 1190 cm^{-1}, and (c) 1135 cm^{-1}. The subtracted spectra were corrected for the argon-induced red-shifts, and an arrow in (a) denotes the signature position of the AA water molecule bend.

argon atoms. It is important to emphasize that, while the empirically determined isomer formation behavior is quite useful for this spectroscopic application, the suppression of the more weakly bound isomer by argon solvation is a curious phenomenon. In the spectra of the larger $(D_2O)_n^-$ clusters, for example, it was observed that creation of the clusters under colder source conditions led to preferential formation of **II**.[10] Thus, although one would suspect that larger argon clusters would lead to colder $(D_2O)_6^-$ core ions, these heavily solvated clusters are, in fact, the species that only display the more strongly bound isomer **I**. Therefore, it may be that the isomer ratio is directed in some dynamical way such that the presence of many Ar atoms somehow suppresses the formation of the more weakly bound isomer, perhaps by inhibiting network rearrangement[20] or even blocking the electron-binding site.

III.2. Vibrational Spectroscopy: Argon Dependence of the $(D_2O)_6^-\cdot Ar_m$ Intramolecular Bending Spectra. Figure 3 presents vibrational predissociation spectra of the $(D_2O)_6^-\cdot Ar_m$ (m = 2, 3, 6, 8, 10) clusters in the 1050−1350 cm^{-1} range covering the DOD intramolecular bending vibrations. No photofragmentation was observed for m = 1, most likely because, with only a single Ar initially present, the nascent $(D_2O)_6^-$ daughter ion is unstable with respect to electron autodetachment. We begin the discussion with the m = 10 spectrum (Figure 3b), as this reflects a dominant contribution from isomer **I** according to its photoelectron spectrum (Figure 2a). The dotted line indicates the location of the bending origin in an isolated D_2O molecule, and like the situation recently reported in the $(H_2O)_6^-$ spectra,[16] one isolated feature (labeled AA in Figure 3a) is observed significantly red-shifted from this location in the m = 10 spectrum (Figure 3b). In fact, the pattern of three bands is quite reminiscent of that displayed by $(H_2O)_6^-$, and to illustrate this point, we have rescaled the $(H_2O)_6^-$ spectrum by a factor of 0.739 in Figure 3a, which is the ratio of the bending fundamental in isolated D_2O to that of H_2O. After scaling, the three bands appear with a very similar spacing and intensity distribution, establishing that isomer **I** in $(D_2O)_6^-$ indeed conforms to the same structure as that found earlier in the $(H_2O)_6^-$ cluster.

As Ar atoms are removed from the m = 10 cluster, a new band emerges at 1175 cm^{-1} (labeled II in Figure 3c), coinciding with the increasing contribution of isomer **II** in the photoelectron spectra (Figure 2). Note that the intensity of the previously identified AA band at 1135 cm^{-1} does not vary with the appearance of the 1175 cm^{-1} feature, but rather closely tracks the intensity of the 1190 cm^{-1} band associated with isomer **I**. This immediately implies that isomer **II** does not contain the AA bending transition. Interestingly, after the 1175 cm^{-1} band, assigned to **II**, is fully developed at m = 6, *another* band appears at lower energy (1163 cm^{-1}) in the m = 3 and 2 spectra. Possibilities for this band's origin include the contribution from yet a third isomer, or more likely, a hot band arising from members of the ensemble retaining more internal energy with fewer attached Ar atoms.

Because of mass degeneracies, it is also conceivable that the $(D_2O)_2^-\cdot Ar_m$ complexes contribute to the vibrational spectra, as they did in the photoelectron spectra (* in Figure 2). However, this possibility could be ruled out by generating a cluster ion beam that only contained the dimer series using a very dilute mixture of water in the source. Ions created under this source condition do not display any predissociating transitions in the entire 1000−4000 cm^{-1} range, as expected for a case where the upper vibrational levels lie far above a cluster's VDE (400 cm^{-1} for n = 2).

III.3. Isolation of the Isomer II Spectrum by Spectral Subtraction. To deconvolute the overlapping spectral signatures of the two primary isomers, we take advantage of the fact that each isomer contributes a set of correlated peaks to the overall observed spectrum. A transparent scheme for extracting the spectrum of isomer **II** from one that includes overlapping contributions from both isomers (e.g., m = 6) is to simply subtract out the spectrum of **I**, isolated in the m = 10 spectrum, from that of the mixture. It is important to correct the spectra prior to subtraction for the solvation shifts in the bands, which are largely peak-independent and on the order of 0.37 cm^{-1}/Ar. A set of subtracted spectra for the m = 6 and 10 pair are

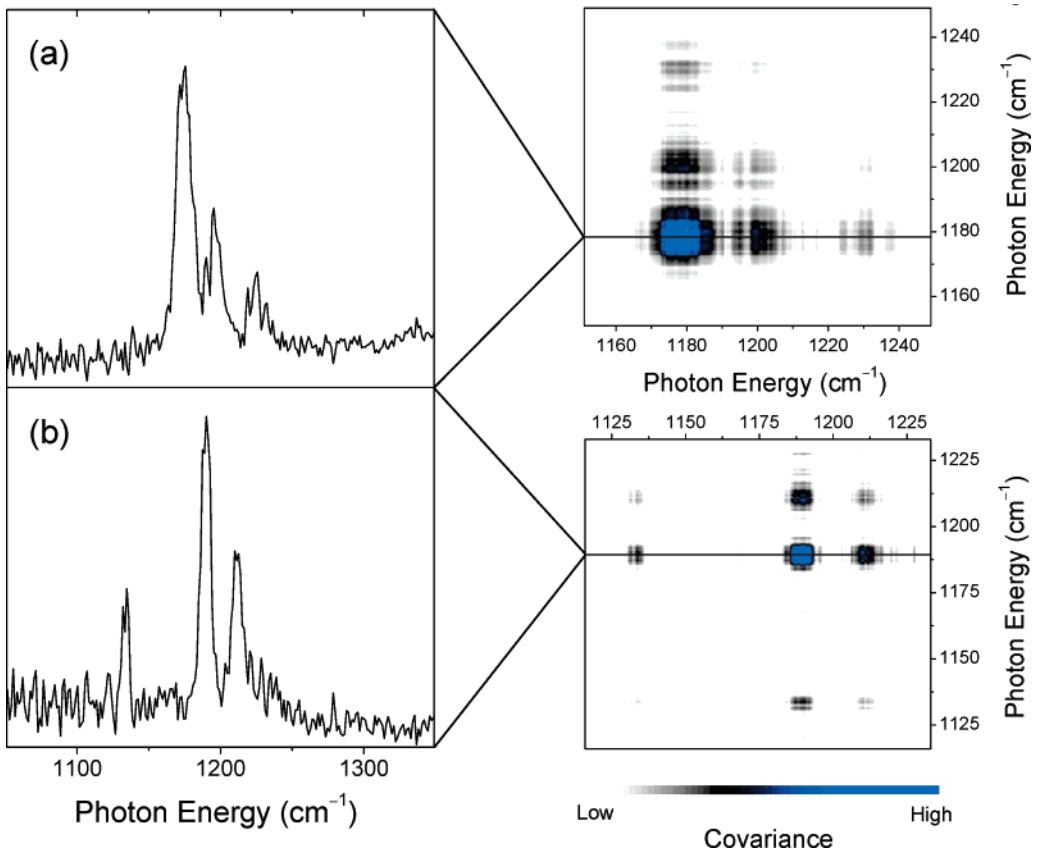

Figure 5. Right panel: covariance maps of $(D_2O)_6^-\cdot Ar_m$ ($m = 6$, 8, 10), normalizing to the 1135 cm^{-1} feature (top) and the 1178 cm^{-1} feature (bottom). Horizontal (and vertical) projections of the maps through the largest feature on the diagonal yield (a) the spectrum of isomer **II** and (b) the spectrum of isomer **I**. In all cases, the spectra were corrected for the argon-induced red-shift.

presented in Figure 4, illustrating that the residual spectrum obtained after subtraction of that due to **I** is independent of the choice of normalization peak (i.e., among the three distinct features in the **I** spectrum). Similar results are obtained when the $m = 8$ and 10 spectra are used to carry out the subtraction. The important conclusion here is that the isomer **II** spectrum does not display the red-shifted signature band of a water molecule in an AA binding site (arrow in Figure 4a). Its dominant band falls quite close to the band origin of the isolated D_2O bend fundamental, as would be expected for water molecules in AD or AAD binding sites. This observation, in turn, implies that the excess electron in **II** is attached to only one dangling OH group from each of the water molecules involved in the supporting network.

III.4. Implementation of Spectral Subtraction with Covariance Mapping. Clearly, one can envision improving the signal-to-noise of the isolated isomer **II** spectrum by extending the subtraction scheme outlined above to all of the spectra. One can, however, carry out a systematic manipulation of the data set that efficiently includes contributions from all such pairwise subtractions using a covariance mapping technique.[21−23] In this approach, the observed infrared spectrum for the $(D_2O)_6^-\cdot Ar_m$ cluster, $S_m(\nu)$, is expressed as a linear superposition of the spectra arising from the independent isomers (i), $S_i(\nu)$, weighted by the m-dependent fractional contribution of each isomer, $f_{i,m}$

$$S_m(\nu) = \sum_i f_{i,m} S_i(\nu) \qquad (2)$$

When we have a series of such spectra that sample a wide range of fractional distribution functions $f_{i,m}$, the independent patterns can be revealed in the two-dimensional covariance map

$$I(\nu_x, \nu_y) = \frac{1}{k} \sum_m [S_m(\nu_x) - S_{\text{avg}}(\nu_x)][S_m(\nu_y) - S_{\text{avg}}(\nu_y)] \qquad (3)$$

where k is the number of independently measured spectra and S_{avg} is the intensity at energy ν_j averaged over all m, the number of attached Ar atoms. When the spectra contributing to the map are normalized to a particular peak, the map can be used to systematically extract all other activity in the spectrum that is linked (i.e., covariant) with this peak.

Two selected covariance maps involving contributions from the $m = 6$, 8, and 10 spectra are included on the right side of Figure 5, where the top map results from normalization of all three spectra to equalize the magnitudes of their AA features, and the bottom map is obtained by normalization to the 1175 cm^{-1} band (II in Figure 3c). The individual spectra were corrected to account for the small shifts induced by Ar (0.37 cm^{-1}/Ar) in order to align the peaks prior to analysis. The utility of the map for spectral deconvolution is that a projection taken along the x- or y-axis through a particular peak on the diagonal yields a trace displaying all other peaks whose intensities are linked to this selected peak. Normalization to a peak arising from a particular isomer thus effectively freezes all of the contributions associated with that species. As such, selection of the distinct AA feature associated with isomer **I** yields the best isolation of the **II** spectrum. Note that this procedure *necessarily* removes an AA contribution from isomer **II**, which we deduced was not a feature of the **II** spectrum on the basis of traces 4a and 4b.

The left panel of Figure 5 displays the two disentangled spectra from the indicated projections along the abscissas shown

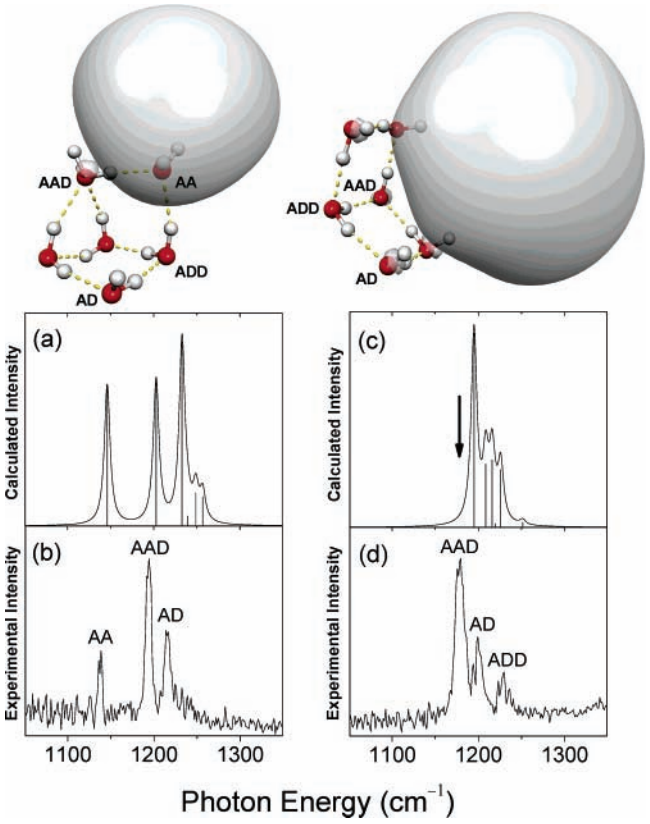

Figure 6. Experimental (from Figure 5, Ar-shift corrected to extrapolate $m = 0$ values) and calculated (scaled to recover the bend in isolated water) bending vibrational spectra of two isomers of the water hexamer anion: (a) calculated armchair, (b) experimental isomer **I**, (c) calculated book, (d) experimental isomer **II**. The armchair (left) and book (right) isomers are included above the spectra, along with a contour of the molecular orbital for the excess electron. The labels A and D describe the numbers of acceptor and donor, respectively, H-bonds associated with a particular water molecule. The arrow in (c) indicates the location of the bend fundamental in isolated D_2O.

on the right. As expected, the lower trace recovers the spectrum of **I** already obtained directly in the $m = 10$ spectrum (Figure 3b), while the upper trace displays the spectrum of **II**. Although, in the present case, we could obtain these traces from a straightforward pairwise subtraction approach, it is useful to establish the equivalence of the covariance method, since it can be applied to more complex situations involving more than two isomers, as well as to less favorable cases where one isomer cannot be directly isolated.

III.5. Implications on the Electron-Binding Motif at Play in Isomer II. To explore the structural implications of the deconvoluted infrared spectra, we turn to electronic structure calculations to identify the expected vibrational patterns associated with the various possible network morphologies. Among the many calculations carried out on small water cluster anions, Kim and co-workers[24] successfully predicted the experimentally observed bending and stretching vibrational spectra of the $n = 4-6$ clusters and indeed identified the crucial role of the AA binding motif. Because those authors only reported the energetics and a few selected frequencies for the $(H_2O)_6^-$ isotopomers, we repeated their B3LYP calculations in order to recover the calculated (harmonic) bending spectra of the $(D_2O)_6^-$ isomers.[24,25] The results are compared to the experimental spectra in Figure 6. The armchair structure assigned[16] to **I** is included at the top of Figure 6, along with its calculated and observed bending spectra for the deuterium isotopomer. The dominant 1190 cm^{-1} transition in the **I** spectrum is traced to a bending fundamental largely involving the embedded AAD water molecule with a dangling hydrogen facing toward the electron, while the AA water molecule (that primarily binds to the excess electron) accounts for the strongly red-shifted feature at 1135 cm^{-1}.

Kim and co-workers[24] also considered the structure of the more weakly bound isomer and concluded that the likely candidate, on the basis of the calculated stability and agreement of its predicted VDE (800 cm^{-1}) with that found experimentally (1500 cm^{-1}), would involve a "book"-type framework illustrated in the right panel of Figure 6. This structure indeed meets our primary experimental criterion that none of its water molecules reside in an AA binding site. As expected, the book structure shown in the right panel does not display any bands on the low-energy side of the bend fundamental in isolated D_2O (arrow in Figure 6c), consistent with the experimental observation. The dominant band of the book, which occurs about 10 cm^{-1} below the AAD band of **I**, is also calculated to arise mostly from the AAD molecule in **II**, but involves substantial displacement of the two flanking AD water molecules as well. The higher-energy bands are then due to the four AD molecules, with the unique ADD water molecule yielding the highest-energy band. Thus, the general character of the spectrum lends strong support for the structural assignment of isomer **II** to the open arrangement predicted by Kim and co-workers.[24] Note that in this book structure, the electron is bound by the combined action of five dangling hydrogen atoms, all arising from different water molecules in the network, rather than to a single AA water molecule that is the signature binding motif for isomer **I**.

Conclusions

A combined photoelectron spectroscopy and infrared predissociation spectroscopy study of argon-solvated water hexamer anions has revealed that fundamentally different local electron-binding motifs are at play in the two experimentally observed isomers of the water hexamer anion. The isomer (**I**) that binds the electron most strongly features one water molecule facing directly into the electron cloud with both hydrogen atoms and is attached to the supporting network in a double H-bond acceptor (AA) site. The isomer (**II**) that binds the electron more weakly displays a different vibrational signature that suggests an alternative binding motif where several water molecules, each residing in AD binding sites, orient their single dangling H atoms toward the excess electron orbital. An important issue to be addressed is to what extent the main persistent difference between isomers **I** and **II** in the large size regime arises from the local binding differences evident at $n = 6$. In particular, it would seem that, in addition to the surface/internal differentiation stressed by Verlet et al.[10] for clusters above $n \approx 50$, there is also a possibility that both **I** and **II** remain surface states even in moderately large clusters but feature different local electron attachment modalities. Note that this scenario would also rationalize the different relaxation dynamics displayed by the two isomer classes as a consequence of the local H-bond topology rather than the overall accommodation morphology.

Acknowledgment. We gratefully acknowledge the Department of Energy for support of this work under grant DE-FG02-00ER15066, as well as discussions with Prof. K. D. Jordan regarding the role of argon in directing the isomer selection branching ratio.

References and Notes

(1) Haberland, H.; Schindler, H.-G.; Worsnop, D. R. *Ber. Bunsen-Ges. Phys. Chem.* **1984**, *88*, 271.

(2) Haberland, H.; Langosh, H.; Schindler, H.-G.; Worsnop, D. R. *J. Phys. Chem.* **1984**, *88*, 3903.

(3) Haberland, H.; Ludewigt, C.; Schindler, H.-G.; Worsnop, D. R. *J. Chem. Phys.* **1984**, *81*, 3742.

(4) Hart, E. J.; Boag, J. W. *J. Am. Chem. Soc.* **1962**, *84*, 4090.

(5) Farhataziz, Rodgers, M. A. J., Eds.; *Radiation Chemistry*; VCH Publishers: New York, 1987.

(6) Arnold, S. T.; Eaton, J. G.; Sarkas, H. W.; Bowen, K. H. In *Ion and Cluster Ion Spectroscopy and Structure*; Maier, J. P., Ed.; Elsevier: Amsterdam, 1989; p 417.

(7) Coe, J. V.; Lee, G. H.; Eaton, J. G.; Arnold, S. T.; Sarkas, H. W.; Bowen, K. H.; Ludewigt, C.; Haberland, H.; Worsnop, D. R. *J. Chem. Phys.* **1990**, *92*, 3980.

(8) Kim, J.; Becker, I.; Cheshnovsky, O.; Johnson, M. A. *Chem. Phys. Lett.* **1998**, *297*, 90.

(9) Shin, J.-W.; Hammer, N. I.; Headrick, J. M.; Johnson, M. A. *Chem. Phys. Lett.* **2004**, *399*, 349.

(10) Verlet, J. R. R.; Bragg, A. E.; Kammrath, A.; Cheshnovsky, O.; Neumark, D. M. *Science* **2005**, *307*, 93.

(11) Lee, G. H.; Bowen, K. H. *J. Korean Phys. Soc.* **2000**, *37*, 76.

(12) Barnett, R. N.; Landman, U.; Cleveland, C. L.; Jortner, J. *Chem. Phys. Lett.* **1988**, *145*, 382.

(13) Weber, J. M.; Kim, J.; Woronowicz, E. A.; Weddle, G. H.; Becker, I.; Cheshnovsky, O.; Johnson, M. A. *Chem. Phys. Lett.* **2001**, *339*, 337.

(14) Paik, D. H.; Lee, I.-R.; Yang, D.-S.; Baskin, J. S.; Zewail, A. H. *Science* **2004**, *306*, 672.

(15) Pshenichnikov, M. S.; Baltuška, A.; Wiersma, D. A. *Chem. Phys. Lett.* **2004**, *389*, 171.

(16) Hammer, N. I.; Shin, J.-W.; Headrick, J. M.; Diken, E. G.; Roscioli, J. R.; Weddle, G. H.; Johnson, M. A. *Science* **2004**, *306*, 675.

(17) Posey, L. A.; Johnson, M. A. *J. Chem. Phys.* **1988**, *89*, 4807.

(18) Posey, L. A.; DeLuca, M. J.; Johnson, M. A. *Chem. Phys. Lett.* **1986**, *131*, 170.

(19) This identification is supported by the variation in intensity of this feature, which mimics the relative mass spectral intensities of $(D_2O)_2^-\cdot Ar_m$ when created in the absence of the hexamer.

(20) Myshakin, E. M.; Diri, K.; Jordan, K. D. *J. Phys. Chem. A* **2004**, *108*, 6758.

(21) Frasinski, L. J.; Codling, K.; Hatherly, P. A. *Science* **1989**, *246*, 1029.

(22) Noda, I. *Appl. Spectrosc.* **1993**, *47*, 1329.

(23) Card, D. A.; Wisniewski, E. S.; Castleman, A. W. *Int. J. Mass Spectrom.* **2003**, *223*, 355.

(24) Lee, H. M.; Lee, S.; Kim, K. S. *J. Chem. Phys.* **2003**, *119*, 187.

(25) Frisch, M. J.; Trucks, G. W.; Schlegel, H. B.; Scuseria, G. E.; Robb, M. A.; Cheeseman, J. R.; MontgomeryJr., J. A.; Vreven, T.; Kudin, K. N.; Burant, J. C.; Millam, J. M.; Iyengar, S. S.; Tomasi, J.; Barone, V.; Mennucci, B.; Cossi, M.; Scalmani, G.; Rega, N.; Petersson, G. A.; Nakatsuji, H.; Hada, M.; Ehara, M.; Toyota, K.; Fukuda, R.; Hasegawa, J.; Ishida, M.; Nakajima, T.; Honda, Y.; Kitao, O.; Nakai, H.; Klene, M.; Li, X.; Knox, J. E.; Hratchian, H. P.; Cross, J. B.; Adamo, C.; Jaramillo, J.; Gomperts, R.; Stratmann, R. E.; Yazyev, O.; Austin, A. J.; Cammi, R.; Pomelli, C.; Ochterski, J. W.; Ayala, P. Y.; Morokuma, K.; Voth, G. A.; Salvador, P.; Dannenberg, J. J.; Zakrzewski, V. G.; Dapprich, S.; Daniels, A. D.; Strain, M. C.; Farkas, O.; Malick, D. K.; Rabuck, A. D.; Raghavachari, K.; Foresman, J. B.; Ortiz, J. V.; Cui, Q.; Baboul, A. G.; Clifford, S.; Cioslowski, J.; Stefanov, B. B.; Liu, G.; Liashenko, A.; Piskorz, P.; Komaromi, I.; Martin, R. L.; Fox, D. J.; Keith, T.; Al-Laham, M. A.; Peng, C. Y.; Nanayakkara, A.; Challacombe, M.; Gill, P. M. W.; Johnson, B.; Chen, W.; Wong, M. W.; Gonzalez, C.; Pople, J. A. *Gaussian 03*; Gaussian, Inc.: Pittsburgh, PA, 2003.